

Fabrication of Zr-Ni Mesoporous Silica Nanocomposites via Consecutive In-Situ Electrolysis for Carbon Dioxide Reforming of Methane

S.M. Sidik^{a*}, A.A. Jalil^b, N.H.R. Anuar^c, N. Hashim^a, M.S. Rosmi^a

^aDepartment of Chemistry, Faculty of Science and Mathematics, Universiti Pendidikan Sultan Idris, 35900 Tanjung Malim, Perak, Malaysia

^bSchool of Chemical and Energy Engineering, Faculty of Engineering, Universiti Teknologi Malaysia, 81310 UTM Johor Bahru, Johor, Malaysia

^cDepartment of Chemistry, Faculty of Applied Science, Universiti Teknologi Mara (UITM) Johor, Pasir Gudang Campus, 81750 Masai, Johor, Malaysia.

*Corresponding Author: smunirah@fsm.upsi.edu.my

Article history :

Received 17 April 2022

Accepted 20 June 2022

ABSTRACT

Hydrogen production via carbon dioxide reforming of methane (CRM) is a promising technology in solving the environmental problems and global energy. Development of a highly efficient, low-cost and stable catalysts seem to be crucial in accelerating its commercialization. In this study, a bimetallic Zr-Ni catalyst supported on MSN (Zr-Ni/MSN) was successfully prepared via consecutive in-situ electrolysis method. An investigation on the physicochemical properties was conducted using XRD, FESEM-EDX, N₂ adsorption-desorption, and CO₂-TPD analyses. The XRD results prove the successful incorporation of Ni and Zr in the MSN catalysts, and the calculated size of Ni particles were decreased upon the sequential addition of Zr into the catalyst. FESEM and EDX elemental mapping analyses showed that, uniform distribution of spherical MSN particles was distorted to a greater extent upon the addition of Zr in the Zr-Ni/MSN catalyst, due to the formation coral-like mesoporous structure and pyramidal Zr-Ni metal structure. While, N₂ physisorption and CO₂-TPD analyses demonstrated that Zr promoter increased the textural properties and basicity of the catalyst. In the CRM, the Zr-Ni/MSN exhibited highest activity up to 97.6% CH₄ conversion and stability up to 50 h time on stream. The pyramidal structure of Ni-Zr was responsible in promoting better properties in the catalyst, thus led to a higher catalytic activity.

Keywords: nickel; zirconia; mesoporous silica; CO₂ reforming of CH₄; in-situ electrolysis

© 2022 School of Chemical and Engineering, UTM. All rights reserved
| eISSN 0128-2581 |

1. INTRODUCTION

The fast depletion of known reserves of fossil fuel is expected to cause energy shortages in the near future [1]. On the other hand, recent studies have been focused on a cleaner and more sustainable ways for energy attaining process to reduce global warming [2]. A dwindling fossil-fuel reserves and worsen climate change phenomena has driven more attention paid to holistic waste management strategies that can utilize waste to produce valuable fuel. Catalytic carbon dioxide reforming of methane (CRM) seems to be a promising route for efficient transformation of two potent greenhouse gases to produce synthesis gas, which can be used as a feedstock for renewable hydrogen or liquid hydrocarbon through the Fischer-Tropsch process [3].

Great efforts have been devoted to develop a suitable catalyst for this reaction. Nowadays, Ni based catalysts have received huge attention and are often chosen as the suitable metal for CRM due to it being more economic and able to

produce high catalytic performances [4]. However, Ni-based catalyst deactivated rapidly at high temperature (more than 600 °C) owing to the Ni sintering and carbon deposition, which impedes the pace to its commercial utilization [5]. Therefore, considerable efforts have been put on exploring ways to development excellent Ni based with good thermal stability and low coke deposition.

Sidik et al., proved that Ni loaded on mesoporous silica nanoparticles (MSN), Ni/MSN prepared by in-situ electrolysis method significantly affected the catalyst's properties and showed better catalytic performance in DRM compared to the commercially used silica support MCM-41 [6]. The support nature able to assist the gasification of carbon species on the surface of Ni due to the presence of suitable amount of Lewis basicity. In addition, Sidik et al, confirmed that developing bimetallic Ni-Co catalysts is a practical method to boost the activity by increasing the nickel dispersion and minimize metal sintering due to intimate contact between nickel and other metal combined

in the bimetallic system [7]. However, the ability of this catalyst in minimizing coke deposition is still under investigation.

One of the major methods which can reduce coking efficiently is through the addition of promoter on the catalyst. Various metal oxide promoter such as CaO, CeO₂, CuO, La₂O₃, MgO and ZrO₂ able to improve coke-resistant ability of Ni-based catalyst [8]. Among all, ZrO₂ is found to be an outstanding promoter owing to its high thermal stability and strong coke inhibitor properties due to its high oxygen vacancies that promote the carbon removal from metallic Ni surfaces [9]. Abdullah et al, studied different ratio of Zr promoter loaded on Ni/SBA-15 via sol-gel hydrothermal method and found that 1Zr/5Ni/SBA-15 is the optimum catalyst for DRM at 800 °C with 50 mL/min inlet reactants [10]. Whereas, Okutan et al., investigated a series of Ni-M (M= Al, Ti and Zr) loaded on mesoporous SBA-15 via one-pot hydrothermal method [4].

It is interesting to note that, there is no literature reported on the influence of Zr promoter on structural properties of Ni loaded on MSN prepared via consecutive in-situ electrochemical method for DRM. Thus, in this current study, the influence of Zr promoter loaded on the Ni/MSN via consecutive in-situ electrochemical method toward its physicochemical properties and DRM were investigated.

2. EXPERIMENTS

2.1 Synthesis of mesoporous silica nanoparticles (MSN)

MSN was prepared by co-condensation and sol-gel method as previously reported [11]. In brief, the cetyltrimethylammonium bromide (CTAB, Merck), ethylene glycol (EG, Merck) and ammonium (NH₄OH, QRec) solution were dissolved in 700 mL of double distilled water with the following mole composition of CTAB:EG:NH₄OH:H₂O=0.0032:0.2:0.2:0.1. After vigorous stirring for about 30 min at 50 °C, 1.2 mmol tetraethylorthosilicate (TEOS, Merck) and 1 mmol 3-aminopropyl triethoxysilane (APTES, Merck) were added to the clear mixture to give a white suspension solution. This solution was then stirred for another 2 h at 80 °C, and the as-synthesized MSN was collected by centrifugation at 20,000 rpm. The as-synthesized MSN was dried at 110 °C and calcined at 550 °C for 3 h to form surfactant-free MSN.

2.2 Preparation of Zr-Ni supported on MSN (Zr-Ni/MSN)

In this study, the Zr-Ni/MSN was prepared by consecutive in-situ electrochemical method, following the procedures reported by [7]. First in-situ electrolysis was conducted to prepare a 2.5wt% Ni/MSN. After calcination at 550 °C for 3 h, a silver colored Ni/MSN was obtained. Then, a consecutive in-situ electrolysis was carried out to dope the second metal, Zr into the Ni/MSN to give 2.5%Zr-

2.5wt%Ni/MSN (Zr-Ni/MSN). As a reference, 5 wt. % of the monometallic Zr/MSN and Ni/MSN were also prepared.

2.3 Characterization

The physicochemical properties of the catalysts were examined by XRD, FESEM-EDX, N₂ physisorption and CO₂-TPD analyses. The XRD was carried out using powder diffractometer (Bruker Advance D8, 40 kV, 40 mA) using a Cu K α radiation source in the range of $2\theta = 1.5-80^\circ$. The crystallite size of NiO (d_{NiO}) was calculated by means of the Scherrer equation. The morphology was observed by FESEM-EDX spectrometer (JSM-6710F). N₂ physisorption isotherms was used to determine the textural properties at liquid nitrogen temperatures using a Beckman Coulter SA 3100 Surface Area Analyzer. CO₂-temperature programmed desorption (CO₂-TPD) analysis was carried out using a flow system equipped with a thermal conductivity detector by Thermo Scientific TPDR1100 flow apparatus. Prior to the experiment, the sample was pretreated at 800 °C for 1h in 5% H₂/Ar mixture. Subsequently, the sample was treated with He for 2h to remove all chemisorb H₂. Then, it was cooled down to 50 °C. 10 pulses of CO₂ (99.9 %) were introduced by an electro-actuated valve with a volume of 0.4 mL. The sample was purged with He to remove the weakly absorbed CO₂. Then, the sample was heated again from 50-900 °C at a heating rate of 10 °C/min in He flow, the desorbed CO₂ was monitored by a TCD detector.

2.4 Catalytic testing

The catalytic CO₂ reforming of CH₄ was performed in a fixed-bed continuous flow reactor at 400-800 °C. Prior to the reaction, 0.2 g of the catalyst was treated by H₂ (50 mL min⁻¹) at 850 °C for 3 h. Then, the reactor was cooling down to a reaction temperature under N₂ stream. CO₂ and CH₄ were mixed at a stoichiometric ratio of 1:1 and N₂ was added as the carrier gas. The reactants with space velocity around 15,000 mL g⁻¹h⁻¹ was passed over the treated catalyst and the products were analyzed using online 6090N Agilent Gas Chromatograph equipped with Carboxen 1010 packed column and TCD detector. The CH₄ conversion was calculated according to the following terms:

$$X_{CH_4} = \frac{[CH_4]_{in} - [CH_4]_{out}}{[CH_4]_{in}} \times 100 \quad (1)$$

where $[CH_4]_{in}$ and $[CH_4]_{out}$ are the molar concentration of CH₄ in the feed and effluent, respectively.

3. RESULTS AND DISCUSSION

Fig. 1 shows the XRD patterns for MSN, ZrO₂, NiO, Ni/MSN, Zr/MSN and Zr-Ni/MSN. Low-angle XRD pattern (Fig. 1A) of MSN, Ni/MSN, Zr/MSN and Zr-Ni/MSN exhibited three distinct peaks at $2\theta = 2.35, 4.05$ and 4.75° , which can be assigned to (100), (110), and (200) reflections of a hexagonal mesoporous structure ($p6mm$) of

the MSN [11]. The intensity of these peaks slightly decreased for Ni/MSN and Zr/MSN, indicating a slight distortion of the ordered mesoporous structure after the modification. However, a significant decrease in intensity was observed for Zr-Ni/MSN, demonstrating a greater distortion of the structure. Since the MSN is not crystalline at the atomic and molecule levels, no reflection was observed at higher angles.

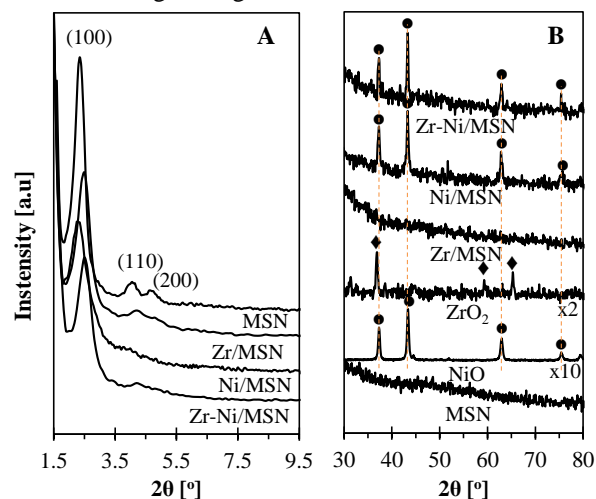


Fig. 1 (A) Low and (B) wide angle of XRD spectra for MSN, Ni/MSN, Zr/MSN, Zr-Ni/MSN, ZrO₂ and NiO. The (●) and (◆) indicated the presence of NiO and ZrO₂ species, respectively.

As shown in Fig. 1B, the NiO, Ni/MSN and Zr-Ni/MSN exhibited four diffraction peaks at $2\theta = 37.3, 43.2, 63.1,$ and 75.6° , corresponding to (111), (200), (220), and (311) planes of NiO, respectively (JCPDS 78-0643). The crystal size of NiO in the Ni/MSN and Zr-Ni/MSN calculated using the Scherrer equation is 5.62 and 3.21 nm, respectively. The ZrO₂ exhibited three peaks at $2\theta = 37.5, 59.4,$ and 64.6° , anatase and monoclinic phase of ZrO₂, respectively (JCPDS 42-1467). In the Zr/MSN and Zr-Ni/MSN catalysts, no ZrO₂ characteristic peaks were observed, suggesting that the particles of Zr is highly dispersed on the surface and the size is smaller than the detection limit of XRD device [10]. Even though there is no distinguishable peak of Zr was observed in the wide angle Zr-Ni/MSN, an obvious peak shifting was observed in the low angle XRD at 2.35° . The peak shifting toward higher 2θ for Zr/MSN and Zr-Ni/MSN is probably due to isomorphous substitution caused by the substitution of Si⁴⁺ ions (0.41 \AA) with Zr⁴⁺ cations ($\sim 0.84 \text{ \AA}$) and structure rearrangement of long-range order of MSN upon the Zr addition [9,12]. The presence of peak shifting also indicating formation of solid solution for supported Ni catalyst [13].

Fig. 2 shows FESEM images of the Ni/MSN and Zr-Ni/MSN at different magnifications. The FESEM image of MSN [11] demonstrated the formation of uniform

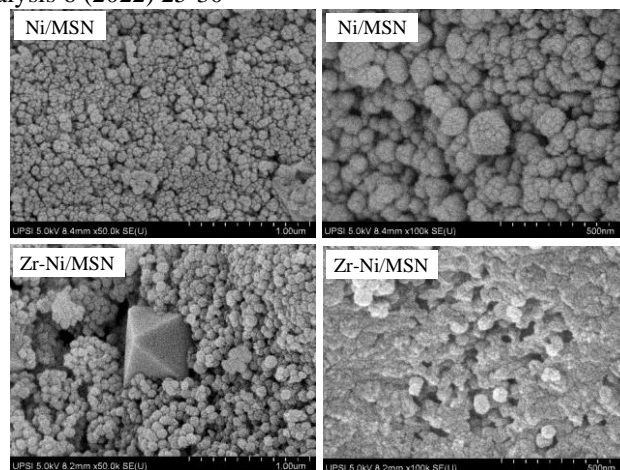


Fig. 2 FESEM images of Ni/MSN and Zr-Ni/MSN at different magnifications.

spherical particles in the size of 40-60 nm. The first in-situ electrolysis process was successful to retain the spherical morphology, but showed an increase in the surface roughness of the catalyst, which is due to the deposition of Ni crystallites [6]. Further addition of Zr in the Ni/MSN catalyst via second in-situ electrolysis process likely seems to disrupt the original MSN's morphology, as the distribution of spherical shape and size is not well uniform, producing a coral-like morphology that have many large holes in between. This may be due to a higher degree of desilication and structural rearrangement of the silica during the consecutive in-situ electrochemical incorporation of the Ni and/or Zr. This observation agrees with the XRD results (Fig. 1A), which revealed that incorporation of the Zr and/or Ni led to distortion in the hexagonal silica order.

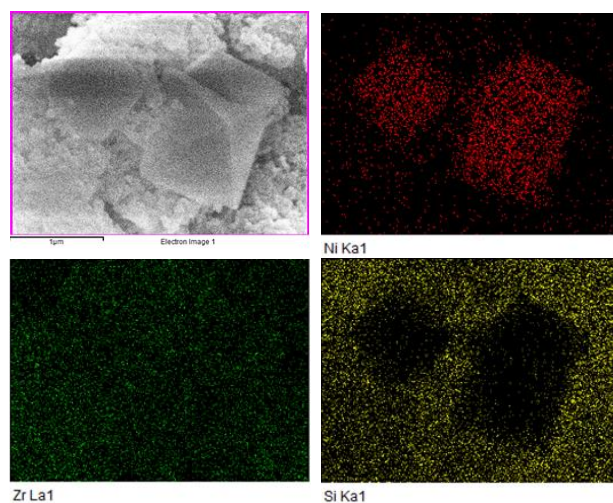


Fig. 3 Elemental mapping analysis of Zr-Ni/MSN.

Interestingly, the Zr-Ni/MSN images showed the existence of new square pyramidal particles. Further EDX-mapping analysis of the pyramidal particles (Fig. 3) elucidated that Zr particles is uniformly distributed on the surface of the catalyst. While Ni particles seemed to dominate the

pyramidal structure area, with the absence of Si particles. This suggested that the Ni and Co particles are located closed to each other at the area of pyramidal structure and possibly might formed an interaction [14].

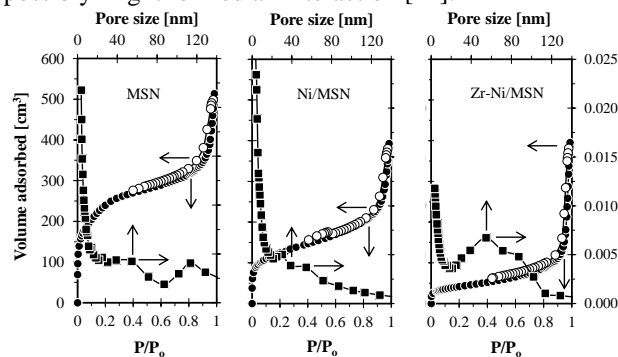


Fig. 4 N₂ adsorption-desorption isotherms and pore size distribution curves for MSN, Ni/MSN and Zr-Ni/MSN.

The textural properties of the MSN, Ni/MSN and Zr-Ni/MSN were determined by N₂ adsorption-desorption analysis. The N₂ adsorption-desorption isotherms and pore size distributions of the catalysts are illustrated in Fig. 4. According to the IUPAC classification, the isotherm of the catalysts exhibited typical Type IV adsorption steps at $P/P_0 = 0-0.1$, $0.3-0.4$, and $0.9-1.0$, which could be classified as a mesoporous material [15]. Although the adsorption steps clearly remained for Ni/MSN and Zr-Ni/MSN, these catalysts showed a remarkable decrease in N₂ adsorption and pore volume compared to the MSN. This indicated that the rearrangement of silica order and pore fillings were occurred during the metal incorporation [16]. In the pore size distributions, all the catalysts demonstrated a bimodal pore structure in the range of 0-20 nm and 20-80 nm. Compared to the MSN, the intensity of pore distribution in both ranges decreased with the addition of Ni or/and Zr. This observation is correlated with the reduction in the quantity of adsorbed N₂ in Ni/MSN at $P/P_0 = 0-0.05$ and $0.9-1.0$, which indicates the reduction of micropores and interparticles void mesopores due to the pore blockage by metal. As for Zr-Ni/MSN, the reduction of micropores in the range of 0-20 nm is even greater which probably caused by a greater pore blockage. Besides, increment of larger pore in the range 20-80 nm was observed, probably due to the increase number of interparticles voids resulted from the new coral-like structure of the MSN (as been shown in Fig.2). In this study, MSN showed the highest surface area and pore volume about $894 \text{ m}^2\text{g}^{-1}$ and $0.979 \text{ cm}^3\text{g}^{-1}$, respectively. The addition of Ni or/and Zr to the MSN resulted in reduction of the surface area and pore volume to 442 and $622 \text{ m}^2\text{g}^{-1}$, and 0.585 and $0.799 \text{ cm}^3\text{g}^{-1}$, respectively. A decrease in surface area and pore volume with the addition of Ni was attributed to partial pore blockage and/or pore filling of the catalysts [17]. In contradiction, consecutive addition of Zr enhanced the texture properties of the catalyst, which can be attributed to increased interparticles voids. This finding is in

accordance to the morphology study that found that coral-like morphology that have many large holes in between.

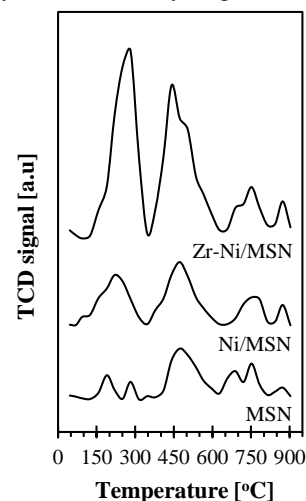


Fig. 5 CO₂-TPD profiles of MSN, Ni/MSN and Zr-Ni/MSN.

To assess the surface basicity of the catalysts, CO₂-TPD analysis were carried out. As shown in Fig. 5, CO₂ was released in two main temperature range reflecting different type of carbonate-like species chemisorb on the surface of the catalyst. In agreement with literature [18], bridged (α species) and bidentate (β species) carbonates desorbed as CO₂ at temperature lower than 250 °C, whereas carboxylate and monodentate carbonates (γ species) desorbed at higher temperature. TPD profile of MSN showed 6 small desorption peaks at 190, 282, 473, 689, 752 and 873 °C. The Ni/MSN showed a greater number of basic sites compared to MSN, distributed in desorption peaks at 251, 504, 783 and 873 °C. While for Zr-Ni/MSN, the highest number of basic sites can be observed from the very sharp peak at 282, 441, 752 and 873 °C. From the analysis, we can see that addition of Ni was successful to improve the mild basic sites, which being assigned around 150-300 °C. Whereas for Zr, it is clearly observed that it can provide large number of mild and strong (more than 400 °C) basic sites to the catalyst. Therefore, the surface basicity of the catalyst can be arranged in the following order: Zr-Ni/MSN > Ni/MSN > MSN. A higher number of basic sites is beneficial to enhance CO₂ adsorption and dissociation.

The initial activity of the catalysts in CRM was studied at different temperature ranging from 400 – 800 °C. A comparative test over MSN is inactive and showed less than 5 % CH₄ conversion even at the highest temperature studied. The activity Ni/MSN and Zr-Ni/MSN are shown in Table 1. As it can be seen, these Ni/MSN and Zr-Ni/MSN demonstrated an increasing trend of CH₄ conversion with increasing temperature and significant activity in the 500-800 °C, as in accordance with the thermodynamic studies of CRM. It is noteworthy that the Zr-Ni/MSN catalysts presented higher conversion than Ni/MSN, suggesting that the smaller Ni particles in Zr-Ni/MSN catalysts could activate more reactants conversion. Moreover, a larger pore

volume and surface area could provide higher accessible site between the active metal and reactants. It is widely accepted that the CH₄ decomposition on the catalyst's active sites is the rate limiting step of the overall process in CRM. Since CH₄ decomposition is a structure-sensitivity reaction, the particle size of the metal has been considered as the key factor to enhance the activity [19]. From the XRD analyses, it was demonstrated that the Ni particle size in Zr-Ni/MSN was slightly reduced and the Ni dispersion was improved with respect to the Ni/MSN. In fact, the small metal particle and better metal dispersion will contribute to more edges and more metal-support structures, and leading to more active sites.

Besides, in the 700 to 800 °C temperature interval, the CH₄ conversion of Zr-Ni/MSN kept higher than the thermodynamic limit values calculated from a direct minimization of Gibbs free energy method using Aspen Plus software [19] and equilibrium data calculated in minimized carbon process condition using DETCHEM software [17]. This result suggest a more intense CH₄ cracking process when CRM is conducted using the Zr-Ni/MSN catalyst under the studied reaction parameters. Stability of Ni/MSN and Zr-Ni/MSN was also tested for 50 h time on stream at 800 °C. Fig. 6 shows the reactants conversion profiles versus time selected.

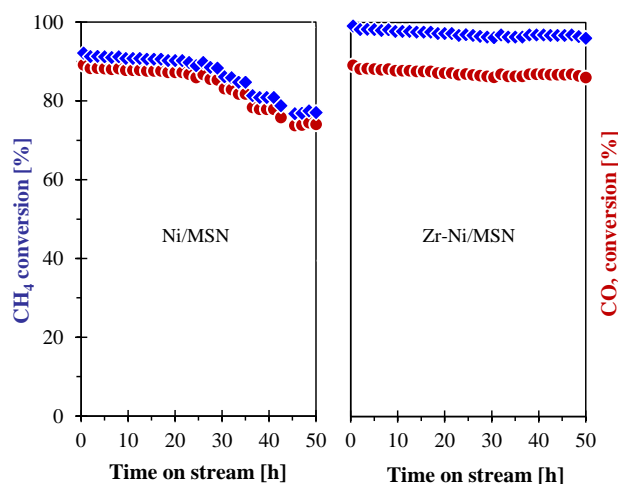


Fig. 6 Evolution of CH₄ and CO₂ conversions with time on stream for Ni/MSN and Zr-Ni/MSN catalysts at 800 °C.

Both Ni/MSN and Zr-Ni/MSN showed a stable CH₄ conversion in 30 h time on stream, but the activity of Ni/MSN started to decrease monotonically earlier compared to Zr-Ni/MSN. This may be due to the homogeneous distribution of Zr on the surface of the catalyst, which is beneficial in preventing the generation of carbon on the Ni surface. This phenomenon promoted a higher CO₂ adsorption and facilitated a greater CO₂ activation, which resulted in the enhancement of carbon elimination by the

reaction of oxygen with carbon intermediate to yield CO [20]. Thus, a lower coke deposit was formed on the catalyst surface and the stability of the catalyst was sustained. As reported by the previous study, the Ni-based catalyst is prone to metal deactivation by sintering and carbon formation [5]. However, in this case, the incorporation of Zr as the promoter in the Zr-Ni/MSN had boosted the activity for a longer period and suppress the carbon formation. From the characterization and catalytic activity results, it can be inferred that synergism occurred between Ni and Zr, where these elements have a mutual role to improve the CRM activity. The interaction formed between Ni and Zr in the pyramidal structure not only able to confine the Ni agglomeration, but also increase the number of Ni-Zr boundaries which could promote oxidation of carbon species formed from the CH₄ dissociation on the Ni metal sites. An illustration of the relationship between particles metal particle size and basicity of Ni-Zr/MSN toward carbon removal inspired by conceptual model established by Huang *et al.*, 2011 [21] and Theofanidis *et al.*, 2016 [22] is depicted in Fig. 7.

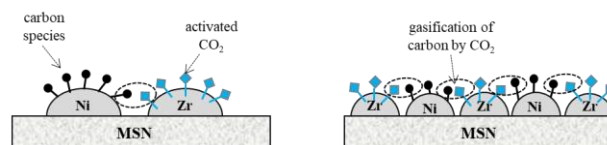


Fig. 7 Conceptual illustration on the relationship of particle size and basicity towards carbon removal.

On a larger metal particle, the carbon species far away from the periphery of the metals tend to nucleate since they cannot reach the activated CO₂. With the increase in time on stream, carbon deposition accumulates in the large particles and cover the metal surface, which results in activity loss [23]. While, for a smaller metal particles, the carbon species derived from the dissociate adsorption of CH₄ near the periphery of the metal particles is easy to react with the activated CO₂ to form CO. While, an increase of basic sites promoted by Zr species enhances the ability of catalyst to adsorb CO₂ in the CO₂ reforming of CH₄. Then, the more adsorbed CO₂ reacts quickly with C species on the Ni surface to form CO. Increased number of Ni-Zr boundaries helps to reduce mass-transfer rate of CO₂ to react with C, and carbon gasification process could proceed as soon as possible, thus reducing coke formation.

Table 1 CH₄ and CO₂ conversion for CRM reaction at different temperatures.

Temperature (°C)	CH ₄ conversion			CO ₂ conversion		
	This study	Equilibrium ^c	Equilibrium ^d	This study	Equilibrium ^c	Equilibrium ^d
500	17.9 ^a , 27.3 ^b	-	-	12.3 ^a , 23.3 ^b	-	-
600	53.6 ^a , 63.5 ^b	-	-	41.6 ^a , 58.1 ^b	-	-
700	77.2 ^a , 93.4 ^b	92	84	74.5 ^a , 86.4 ^b	65	91
800	94.3 ^a , 97.6 ^b	96	95	91.7, 93.7 ^b	88	97

^aExperimental data obtained in this study for Ni/MSN catalyst

^bExperimental data obtained in this study for Zr-Ni/MSN catalyst

^cData reported in [19] based on direct minimization of Gibbs free energy method using Aspen plus software.

^dData reported in [17] based on DETCHEM software in minimized carbon formation process conditions.

4. CONCLUSION

In this study, Zr-Ni/MSN was successfully prepared by a consecutive in-situ electrolysis. XRD analyses demonstrated that the Zr-Ni/MSN has smaller and better dispersion of metal particles with respect to the Ni/MSN. The addition of Zr as the promoter in Zr-Ni/MSN favored the formation of coral-like mesoporous structure nanoparticles and enhance the surface area of the catalyst, as proven by FESEM and N₂ physisorption analyses. EDX elemental mapping suggested that the pyramidal structure is consisted of homogenous dispersion of Zr and Ni, with higher density of Ni particles. The Zr-Ni/MSN catalyst demonstrated excellent performance for CO₂ reforming of CH₄. The synergy effect between Ni and Zr in the catalyst not only provided high activity, but also a better carbon tolerant ability, with a stable performance for more than 30 h time on stream. Lastly, those square pyramidal structures of Ni-Zr could act as a one stop center to the catalyst as it could react in bi-functional mechanism: i) CH₄ dissociation on the Ni metal sites, and ii) CO₂ adsorption and activation by Zr species. It is believed that this work is a great contribution to the development of nano-catalyst for energy production, particularly towards the utilization of harmful greenhouse gases into valuable syngas.

ACKNOWLEDGEMENTS

This work is supported by the Universiti Pendidikan Sultan Idris and Universiti Teknologi Malaysia through Research University Grant no.0147-101-01 and 05H09, respectively. Our gratitude also goes to the Hitachi Scholarship Foundation for the Gas Chromatograph Instrument Grant.

REFERENCES

- [1] D.C. Wilson, Waste Management Research 25 (2007) 198.
- [2] R. G. dos Santos, A.C. Alencar. International Journal of Hydrogen Energy 45 (2020) 18114.
- [3] V. Wells, A. Riaz, Q. Sun, X. Li, N. Yan, C.-H. Wang, W. Lipinski, Applied Physical Letters 120 (2022) 143905.
- [4] C. Okutan, H. Arbag, N. Yasyerli, S. Yasterli. International Journal of Hydrogen Energy 45 (2020) 13911.
- [5] A.H. Fakeeha, A.S. Al-Fatesh, A.A. Ibrahim, A.E. Abasaheed. Journal of Saudi Chemical Society 25 (2021) 101244.
- [6] S.M. Sidik, A.A. Jalil, S. Triwahyono, T.A.T. Abdullah, A. Ripin. RSC Advances 5 (2015) 37405.
- [7] S.M. Sidik, S. Triwahyono, A.A. Jalil, Z.A. Majid, N. Salamun, N.B.

- Talib, T.A.T Abdullah, Chemical Engineering Journal 295 (2016) 1.
- [8] Y. Wang, L. Yao, Y. Wang, S. Wang, Q. Zhao, D. Mao, C. Hu. ACS Catalysis 8 (2018) 6495.
- [9] M. Prasad, K. Ray, A. Sinhamahapatra, S. Sengupta. Journal of Material Sciences 57 (2022) 2839.
- [10] N. Abdullah, N. Ainirazali, H. Ellapan. International Journal of Hydrogen Energy 48 (2021) 24806.
- [11] A.H. Karim, A.A. Jalil, S. Triwahyono, S.M. Sidik, N.H.N. Kamarudin, R. Jusoh, N.W.C. Jusoh, B.H. Hameed. Journal of Colloid and Interface Sciences 386 (2012) 307.
- [12] M.S. Aw, I.G.O. Črnivec, P. Djinić, A. Pintar. International Journal of Hydrogen Energy 24 (2014) 12636.
- [13] L. Pastor-Pérez, E. Le Sache, C. Jones, S. Gu, H. Arellano-Garcia, T.R. Rienna. Catalysis Today. 317 (2018) 108.
- [14] L. Xu, X. Wen, M. Chen, C. Lv, Y. Cui, X. Wu, C. Wu, B. Yang, Z. Miao, X. Hu. Fuel 282 (2020) 118813.
- [15] P. Hongmanom, J. Ashok, S. Das, N. Dewangan, Z. Bian, G. Mitchell, S. Xi, A. Borgna, S. Kawi. Journal of Catalysis 387 (2020) 47.
- [16] L. Lyu, M. Shengene, Q. Ma, J. Sun, X. Gao, H. Fan, J. Zhang, T.-S. Zhao. Fuel 310 (2022) 122375.
- [17] F. Agueniou, H. Vidal, M.P. Yeste, J.C. Hernández-Garrido, M.A. Cauqui, J.M. Rodríguez-Izquierdo, J.J. Calvino, J.M. Gatica. Catalysis Today 383 (2022) 226.
- [18] I. Luisetto, S. Tuti, C. Romano, M. Boaro, E.D. Bartolomeo, J. K. Kasavan, S.M.S. Kumar, K. Selvakumar. Journal of CO₂ Utilization 30 (2019) 63.
- [19] M.K. Nikoo, N.A.S. Amin, Fuel Processing Technology 92 (2011) 678.
- [20] S.S. Miri, F. Meshkani, A. Rastegarpanah, M. Rezaie. Chemical Engineering Science 250 (2022) 116956.
- [21] T. Huang, W. Huang, J. Huang, P. Ji. Fuel Processing Technology 92 (2011) 1868.
- [22] S.A. Theofanidis, R. Batchu, V.V. Galvita, H. Poelman, G.B. Marin. Applied Catalysis B: Environmental 185 (2016) 42.
- [23] Y. Wang, Z. Zhang, S. Zhang, Y. Wang, S. Hu, J. Ziang, T. Wei, S. Niu, X. Hu. Journal of the Energy Institute 101 (2022) 277.